

Characterization of evolution of mode coupling in a graded-index polymer optical fiber by using Brillouin optical time-domain analysis

Yongkang Dong,^{1,*} Pengbai Xu,¹ Hongying Zhang,² Zhiwei Lu,¹ Liang Chen,³ and Xiaoyi Bao³

¹National Key Laboratory of Science and Technology on Tunable Laser, Harbin Institute of Technology, Harbin 150001, China

²Department of Optoelectronic Information Science and Engineering, Harbin University of Science and Technology, Harbin 150080, China

³Fiber Optics Group, Department of Physics, University of Ottawa, Ottawa, K1N 6N5, Canada
*aldendong@gmail.com

Abstract: A narrow bandwidth (2GHz) π -phase-shift flattop fiber Bragg grating (FBG) is proposed to achieve Brillouin optical time-domain analysis (BOTDA) for perfluorinated graded-index polymer optical fibers (GI-POFs) for the first time to best of our knowledge. Using the technique of BOTDA, we explore the evolution of mode coupling in perfluorinated GI-POFs by analyzing the Brillouin frequency shift (BFS) variation along the whole fiber, and compare them with that of silica graded index multimode fibers (GI-MMFs). The characteristics of mode coupling of GI-POFs and GI-MMFs were also investigated in terms of the speckle patterns at the output face of the two fibers. The results show that compared with silica GI-MMFs, GI-POFs exhibit more efficient mode coupling and the excellent ability of mode scrambling regardless of alignment conditions.

©2014 Optical Society of America

OCIS codes: (060.2400) Fiber properties; (250.5460) Polymer waveguides; (290.5900) Scattering, stimulated Brillouin.

References and links

1. S. Loquai, F. Winkler, S. Wabra, E. Hartl, B. Schmauss, and O. Ziemann, "High-speed, large-area POF receivers for fiber characterization and data transmission 10-Gb/s based on MSM-photodetectors," *J. Lightwave Technol.* **31**(7), 1132–1137 (2013).
2. K. Makino, Y. Akimoto, K. Koike, A. Kondo, A. Inoue, and Y. Koike, "Low loss and high bandwidth polystyrene-based graded index polymer optical fiber," *J. Lightwave Technol.* **31**(14), 2407–2412 (2013).
3. M. Matsuura, R. Furukawa, Y. Matsumoto, A. Inoue, and Y. Koike, "Evaluation of modal noise in graded-index silica and plastic optical fiber links for radio over multimode fiber systems," *Opt. Express* **22**(6), 6562–6568 (2014).
4. N. Hayashi, Y. Mizuno, and K. Nakamura, "Brillouin gain spectrum dependence on large strain in perfluorinated graded-index polymer optical fiber," *Opt. Express* **20**(19), 21101–21106 (2012).
5. Y. Mizuno and K. Nakamura, "Potential of Brillouin scattering in polymer optical fiber for strain-insensitive high-accuracy temperature sensing," *Opt. Lett.* **35**(23), 3985–3987 (2010).
6. A. Minardo, R. Bernini, and L. Zeni, "Distributed temperature sensing in polymer optical fiber by BOFDA," *IEEE Photon. Technol. Lett.* **26**(4), 387–390 (2014).
7. Y. Mizuno and K. Nakamura, "Experimental study of Brillouin scattering in perfluorinated polymer optical fiber at telecommunication wavelength," *Appl. Phys. Lett.* **97**(2), 021103 (2010), doi:10.1063/1.3463038.
8. Y. Mizuno, N. Hayashi, and K. Nakamura, "Brillouin scattering signal in polymer optical fiber enhanced by exploiting pulsed pump with multimode-fiber-assisted coupling technique," *Opt. Lett.* **38**(9), 1467–1469 (2013).
9. Y. Mizuno, M. Kishi, K. Hotate, T. Ishigure, and K. Nakamura, "Observation of stimulated Brillouin scattering in polymer optical fiber with pump-probe technique," *Opt. Lett.* **36**(12), 2378–2380 (2011).
10. Y. Mizuno, T. Ishigure, and K. Nakamura, "Brillouin gain spectrum characterization in perfluorinated graded-index polymer optical fiber with 62.5- μ m core diameter," *IEEE Photon. Technol. Lett.* **23**(24), 1863–1865 (2011).
11. N. Hayashi, Y. Mizuno, and K. Nakamura, "Characterization of stimulated Brillouin scattering in polymer optical fibers based on lock-in-free Pump-Probe technique," *J. Lightwave Technol.* **31**(19), 3162–3166 (2013).
12. Y. Mizuno and K. Nakamura, "Core alignment of butt coupling between single-mode and multimode optical fibers by monitoring Brillouin scattering signal," *J. Lightwave Technol.* **29**(17), 2616–2620 (2011).

13. R. W. Boyd, *Nonlinear Optics* (Academic, 2008), Chap. 9.
14. Y. Chen, Z. Lu, Y. Wang, and W. He, "Phase matching for noncollinear Brillouin amplification based on controlling of frequency shift of Stokes seed," *Opt. Lett.* **39**(10), 3047–3049 (2014).
15. V. I. Kovalev and R. G. Harrison, "Waveguide-induced inhomogeneous spectral broadening of stimulated Brillouin scattering in optical fiber," *Opt. Lett.* **27**(22), 2022–2024 (2002).
16. Y. Dong, L. Chen, and X. Bao, "Time-division multiplexing-based BOTDA over 100 km sensing length," *Opt. Lett.* **36**(2), 277–279 (2011).
17. X. Zou, M. Li, W. Pan, L. Yan, J. Azaña, and J. Yao, "All-fiber optical filter with an ultranarrow and rectangular spectral response," *Opt. Lett.* **38**(16), 3096–3098 (2013).
18. B. M. Trabold, D. Novoa, A. Abdolvand, and P. St. J. Russell, "Selective excitation of higher order modes in hollow-core PCF via prism-coupling," *Opt. Lett.* **39**(13), 3736–3739 (2014).

1. Introduction

Perfluorinated graded-index polymer optical fibers (GI-POFs) make an excellent choice for the installation of high-performance fiber networks for its capabilities of combining high data transmission rates [1] and low attenuation [2]. On one hand, compared with silica graded-index multimode optical fibers (GI-MMFs), GI-POFs feature easy handling, low-cost and an inherently higher tolerance to misaligned connection, by which GI-MMFs are easily influenced and appear in transmission performance degradation [3].

On the other hand, thanks to their good characters of high flexibility, capability of a small bending radius and a high sensitivity to temperature, GI-POFs have substantial potential in sensing applications [4–6]. Since Brillouin scattering is a very effective sensing mechanism, the basic Brillouin scattering properties of GI-POFs have been investigated in recent years, including Brillouin gain coefficient, Brillouin threshold power, Brillouin frequency shift (BFS) [7] and its dependences on large strains (>50%) [4] and a high-temperature coefficient (−4.09 MHz/K) [5], these make it possible to sustain a large strain load and high precision temperature sensing. Two useful techniques were proposed to enhance the weak Brillouin scattered light of the GI-POFs: multimode-fiber-assisted coupling technique [8] and pump-probe technique [9]. The fact that the GI-POFs' length has little contribution to the Brillouin gain spectrum (BGS) when it is longer than 50 m is proved [10] and an optimal Stimulated Brillouin Scattering (SBS) observation of 3.8m long GI-POFs was found out [11]. In addition, Brillouin scattered light between silica-based GI-MMFs and GI-POFs with respect to different core alignment positions was investigated experimentally, and the results shown that BFS changes originated from the excitation of higher order modes [12].

However, there are some challenges impeding the implementation of distributed measurement of Brillouin scattering in GI-POFs: firstly, the strong Fresnel reflection caused by index mismatch of different materials at the interface of the silica-based GI-MMFs (~1.46) and GI-POFs (~1.35) will lead to photodiode saturation and hinder the measurement of the weak Brillouin signal [6]; secondly, the BFS (2.83GHz) [7] of GI-POFs is much smaller than that of a silica optical fiber, which largely aggravates the difficulty of separating the Brillouin scattered light from the probe beam; finally, the considerable high loss (150dB/km) of GI-POFs at 1.55 μ m is another challenge for photo detector to fully identify the amplification of the probe beam over a long fiber. Up to now, the only published paper about distributed measurement of Brillouin scattering in GI-POFs is [6], where the technique of Brillouin optical frequency-domain analysis is used, nevertheless, there is no report about Brillouin optical time-domain analysis (BOTDA) to achieve it due to the factors mentioned above.

In this paper, we propose to use a narrow bandwidth (2GHz) π -phase-shift flattop fiber Bragg gating (FBG) to achieve BOTDA for perfluorinated GI-POFs by filtering out the Fresnel reflection mentioned above for the first time to best of our knowledge; furthermore, we also propose a BOTDA-based method to analyze the evolution of mode coupling in perfluorinated GI-POFs by analyzing the BFS changing along the whole fiber. Multimode-fiber-assisted coupling technique is used to avoid the burning or damage at the POF surfaces. The measurements of distributed BFS over the GI-POFs and GI-MMFs have been carried out to analyze the mode coupling and the speckle patterns at output face of two fibers are observed to verify the mode coupling. Different core alignment positions are adjusted to investigate the ability of mode scrambling of the GI-POFs and GI-MMFs.

2. Principle

In a bulk medium, the BFS is defined as

$$v_B = \frac{2nV}{\lambda} \cos\left(\frac{\theta}{2}\right) \quad (1)$$

In Eq. (1), n is the refractive index, V is the sound velocity, λ is the wavelength in vacuum, θ is the crossing angle of the pump and the spontaneous scattered light (or the probe light in a Brillouin amplification system) [13]. Because the bulk medium is homogeneous, V and n are constant; if θ is increased, the BFS will be decreased [14]. In a single-mode fiber, the BFS has a fixed value since there is only the fundamental mode propagating in the fiber and this is determined by the material and the waveguide structure. However, in a multimode fiber, as is shown in Fig. 1, θ depends on NA , which means that Brillouin linewidth broadening would arise from the ability of optical fiber to guide a fan of beam directions within a full angle θ , where $\theta/2$ equals to the critical angle of a fiber, i.e. the waveguide-induced inhomogeneous broadening [15]. With increasing the incident angle of the optical wave, more high-order modes are excited, which will give rise to the variation of BFS. The results in [12] show that the BFS of GI-MMFs will increase with enlarging the offset of core alignment; conversely, this action will cause the BFS of GI-POFs to decrease. The opposite results of BFS variance shown in [12] should be induced by the different velocities of high-order acoustic waves of the two kinds of fiber, so that the variation of the BFS in the GI-MMFs or GI-POFs characterizes the evolution of the mode coupling.

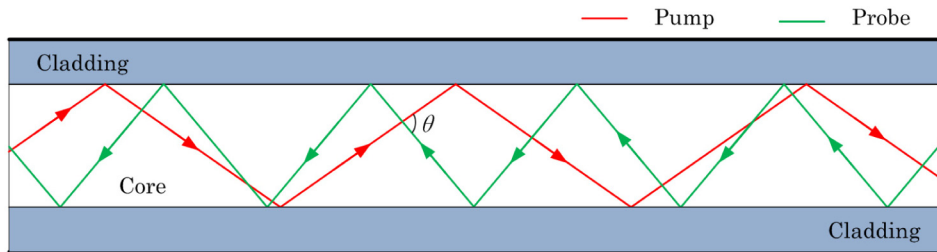


Fig. 1. The scheme of SBS in the GI-POFs.

3. Experiment setup

The experimental setup is illustrated in Fig. 2. All the optical paths are composed of silica SMFs except for the fiber under test (FUT). A 40-m-long perfluorinated GI-POF (Chromis Fiberoptics, Inc.) with numerical aperture of 0.185, core size of 50 μ m, core refractive index of \sim 1.35 and a 40-m-long silica GI-MMF (Corning Inc.) with numerical aperture of 0.24, core size of 62.5 μ m, core refractive index of \sim 1.46 are used as FUT. Noted that the width of the pump pulse used in the experiment is 30ns corresponding to a 3-m spatial resolution in a silica fiber with the index of 1.468, while the index of GI-POF is slightly smaller than that of silica fibers, so the spatial resolution is 3.3m. The peak power of pulse pump is 1.2W and the power of probe is 200mW, which lead to a relative high signal intensity. In order to avoid damage at the surface of GI-POF induced by high-peak-power optical pulse injection, a piece of 50/125 silica GI-MMF is inserted at POF/SMF interface. As is shown in the inset of Fig. 2, one end of GI-MMF is spliced to a standard single mode fiber by arc fusion (both silica glass) and the other end is connected to GI-POF by flange connection.

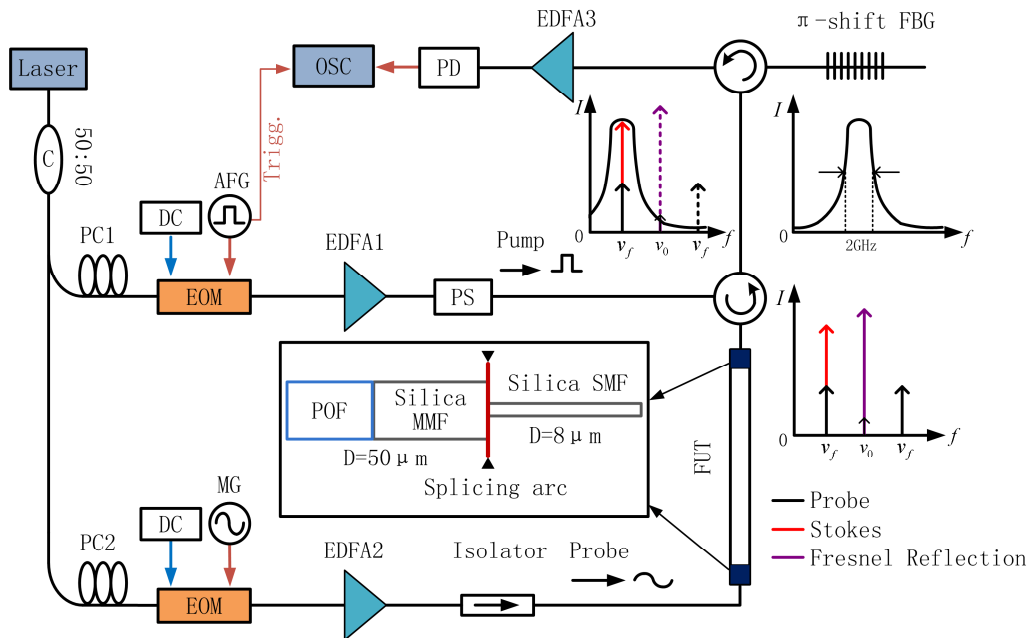


Fig. 2. Experimental setup. C, coupler; PC, polarization controller; EOM, electro-optic modulator; DC, direct current; AFG, arbitrary function generator; MG, microwave generator; EDFA, erbium-doped fiber amplifier; PS, polarization scrambler; FUT, fiber under test; FBG, fiber Bragg grating; PD, photo detector; OSC, Oscilloscope.

The output of an optical fiber laser is split into two arms by a 50/50 coupler providing two waves, i.e. the pump and the probe. An arbitrary function generator is used to drive a high extinction ratio (>45 dB) electro-optic modulators to generate the pump pulse. Before launched into the FUT, the pump pulse is amplified by an erbium doped fiber amplifier (EDFA 1). A polarization scrambler is used to randomly change the polarization state of the pump pulse to reduce the polarization-fading induced fluctuation on the signal by averaging a large number of signal traces, where 500 times averaging is used in our experiment. Similarly, the downshifted probe wave is acquired by modulating the output of the laser, and a BGS can be obtained by scanning the frequency offset between the pump and the probe in the vicinity of the BFS. After amplified by EDFA 2, the probe beam is launched into the FUT. As it is shown at the right side of the FUT, the lower sideband wave of the probe is amplified by the pump wave through stimulated Brillouin scattering interaction. At the same time, the strong Fresnel reflection is introduced at the frequency of the pump wave due to the index mismatching of the two fibers. After accurately adjusting the frequency of the laser, the Stokes signal is located at the transmission band of the 2 GHz π -phase-shift flattop FBG and subsequently is extracted, while the upper sideband of the probe wave and the strong Fresnel reflection of the pump pulse at the interface of the silica and polymer fibers are ultimately suppressed. Since the power of the extracted lower sideband of the probe wave is relatively weak, EDFA 3 is used to amplify the optical wave to the detectable level. Then, the amplified lower sideband was converted into an electrical signal with a photo detector and monitored by an oscilloscope [16]. Note that the bandwidth of a conventional FBG are several tens of GHz or more, which largely exceeds the BFS of GI-POFs and can't play the role of a phase-shift FBG filter with an ultra-narrow bandwidth down to the order of magnitude of MHz [17]. The π -phase-shift FBG of 2GHz narrow bandwidth used can efficiently filter out the strong Fresnel reflection to acquire the Brillouin signal.

4. Experimental results

The typical measured distributed BFS of GI-POF and GI-MMF are shown in Fig. 3(a). The BFS of GI-POF undergoes an irregular and large-scale variance, which changes from 2.792GHz to 2.822GHz with a variation range of 30 MHz. The varying BFS along the fiber indicates that there are a lot of modes in the GI-POF, and considerable mode coupling exists between the lower-order mode and higher-order mode. The evolution of the mode coupling is clearly observed and the spatial period of the mode coupling is a few meters based on the BFS change over the fiber. For comparison, the BFS of silica GI-MMF is measured at the same experimental condition and is also plotted in Fig. 3(a), where the BFS of GI-MMF is around 9.835GHz. Conversely, the curve of BFS in GI-MMF is relatively smooth and the variation along the whole fiber is as low as 2.5MHz, which means that there are fewer modes propagating in the fiber and weak mode coupling to high-order modes compare with that of GI-POF.

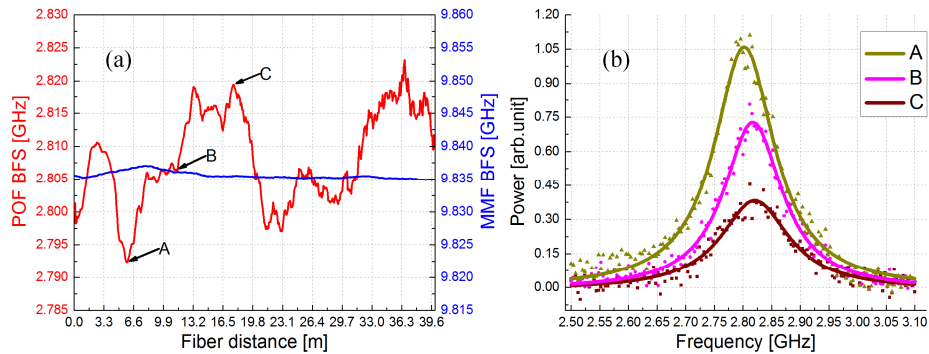


Fig. 3. (a) measured BFS, red curve: polymer fiber, blue curve: silica multimode fiber; (b) measured BGS of point A, B and C marked in (a), the solid lines show the Lorentzian fits.

The BGS of GI-POF at point A, B and C in Fig. 3(a) are shown in Fig. 3(b), which correspond to different BFSs and subsequently different modes. The solid lines show the Lorentzian fits. The decreasing of the power of the BGS from point A to point C mainly originates from the high loss of the GI-POF at 1550nm. In general, the Brillouin bandwidth of GI-POF is 105MHz [4] and its width is closely related to mode coupling. The bandwidth of BGS of point A, B and C is 127 MHz, 123 MHz and 135MHz, respectively, which indicate that there are many modes from point A to point C and hence, mode coupling between the lower-order mode and the higher-order mode. At the same time, we record the power distribution at the output face of the GI-MMF and GI-POF using a CCD on the condition of central alignment as shown in Fig. 6(a1) [18], and the measured power distribution are shown in Fig. 6(b1) and 6(c1). From Fig. 6(b1) we can see that the optical power mainly concentrates in the fundamental and low-order modes in a GI-MMF, while in Fig. 6(c1) the optical power distribution exhibits a speckle pattern indicating that the power is dispersed among a lot of modes in a GI-POF. This phenomenon coincides with the analysis of BFS variation in Fig. 3(a). We believe that the superiority of mode coupling of the GI-POF is mainly caused by the polymer inhomogeneity of the waveguide.

10 separate measurements of BFS have been demonstrated for both GI-POF and GI-MMF to fully investigate the characteristics of mode coupling, respectively. During the measurements, temperature was kept constant and there was no external disturbance to FUT. As is shown in Fig. 4(a), the maximum variation BFS of GI-POF is 35MHz, which is slightly higher than that in Fig. 3(a). In Fig. 4(b), the BFS of GI-MMF varies from 9.833GHz to 9.837GHz with a variation range of 4 MHz, which is nearly one order of magnitude smaller than that of GI-POF. The BFS of GI-POF varies quickly and randomly over the time, which indicates that the mode coupling in the GI-POF changes quickly and disorderly; while for the GI-MMF, the variation is small. The comparison shows that the mode coupling in GI-POF is

stronger than that of GI-MMF. At the same time, we record the power distribution at output face of the GI-POF and the GI-MMF every ten second and the acquired photos are made into animations (see [Media 1](#) and [Media 2](#)). In [Media 1](#), the speckle varies largely over the time and the optical power fluctuate between different modes continuously, which indicate that mode coupling in the GI-POF is strong and unstable; in [Media 2](#), the power mainly concentrate at the central of the core and there is not much shift over the time indicating that mode coupling in the GI-MMF is weak and stable. The phenomenon coincides with the analysis of variation of BFS in Fig. 4. As stated above, these two kinds of fiber are both multimode fiber with nearly the same core diameter, the only difference is the material used, i.e., one is silica and the other is polymer. Therefore, the origin of the exhibited difference is coming from the different materials.

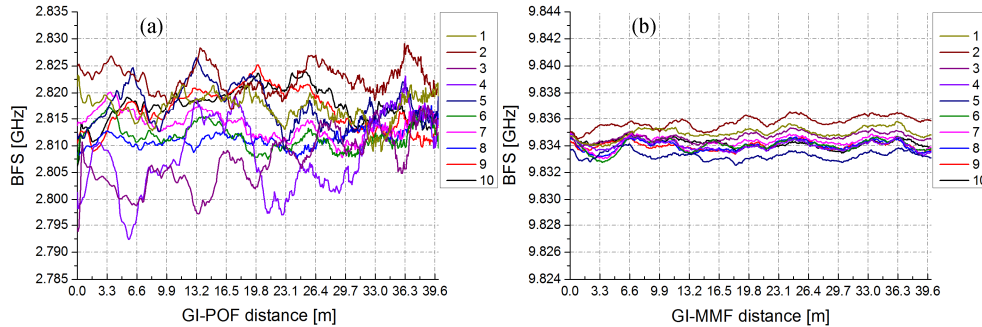


Fig. 4. 10 BFS measurements in (a) a GI-POF (see [Media 1](#)) and (b) a GI-MMF (see [Media 2](#)).

Then, we repeat the BFS measurement with the utmost radial offset of $25\mu\text{m}$ at SMF/MMF interface to purposely excite the high-order modes of the probe wave, the pump wave is centrally launched into the FUT. As is shown in Fig. 5, a disorderly variation from 2.805GHz to 2.830GHz of BFS of GI-POF is observed and a large-scale mode coupling still exists. We can see that the varied range of BGS of GI-POF is almost the same with the former measurements of central alignment, which proves that offset splicing makes little difference to GI-POF on the property of mode scrambling.

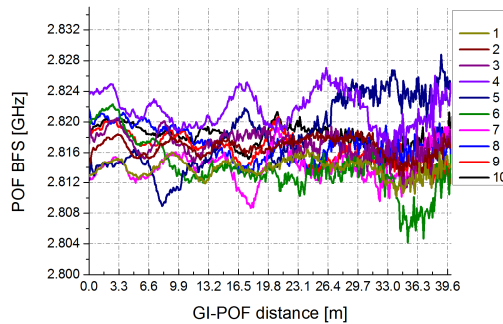


Fig. 5. 10 BGS measurements of a GI-POF under $25\mu\text{m}$ offset splicing at SMF/MMF interface.

To understand the observed phenomena in terms of fiber modes, the speckles at the output face of FUT are monitored for different offsets at the SMF/MMF interface. Different offset splicing positions are acquired by a CCD of fusion splicer in Fig. 6(a) and the photos of speckle of the GI-MMF and GI-POF are shown in Fig. 6(b) and 6(c). Under the condition of central alignment, the speckle of GI-POF is several times larger than that of GI-MMF, while the intensity contrast is more obvious in the GI-MMF than that of GI-POF. Particularly, with increasing the offset, the speckle of the GI-MMF grows bigger quickly with larger attenuation, whereas this action in the GI-POF is different: the lower-order mode and higher-order modes are both excited for different offsets including the central alignment. With

central alignment, GI-MMF can keep mode constant; however, mode distributions will vary once the optical wave is offsetting launched. The irregular fluctuation of optical power between different modes of the three photos in Fig. 6(c) has no significant overall difference, which is the advantage for mode scrambling device of GI-POF to resist misalignment. Hence, GI-POFs have the excellent ability of keeping mode scrambling regardless of alignment condition whereas GI-MMFs are easily influenced. The result confirms that GI-POFs have an inherently higher ability to keep mode scrambling than GI-MMFs.

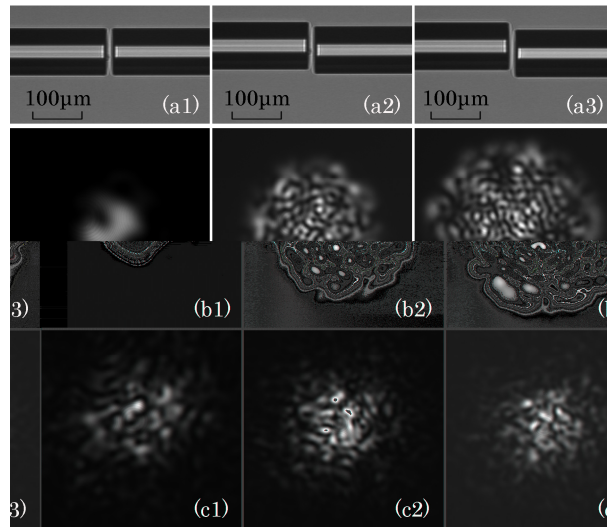


Fig. 6. (a) Different splicing positions acquired by a fusion splicer. Speckle patterns of (b) GI-MMFs and (c) GI-POFs outputs for different offset positions

5. Conclusion

In conclusion, we propose to use a narrow bandwidth (2GHz) π -phase-shift flattop FBG to achieve BOTDA for perfluorinated GI-POFs. Then, we analyze the evolution of mode coupling in perfluorinated GI-POFs and investigate the ability of mode scrambling of the GI-POFs and GI-MMFs. The results show that the evolution of mode coupling in the GI-POFs is more efficient than that of GI-MMFs, which prove that GI-POFs are good mode scrambler with excellent performance to keep mode scrambling. We believe that the origin of the exhibited difference is coming from the intrinsic material non-uniformity of the polymer fiber. This inherent character of mode coupling of GI-POFs can be of great use in the research of mode scrambling device. Subsequent quantitative analysis research about the mode coupling of GI-GOFs is under investigation.

Acknowledgement

The authors would like to acknowledge the financial support from the National High Technology Research and Development Program of China 863 Program 2014AA110401, the National Natural Science Foundation of China 61205073 and 61308004, Foundation for Talents Returning from Overseas of Harbin 2013RFLXJ013, China Postdoctoral Science Foundation 2013M530155, and State Key Laboratory of Advanced Optical Communication Systems and Networks, Shanghai Jiao Tong University, China 2013GZKF031303.